Journal of Power Sources 263 (2014) 223–230

Contents lists available at ScienceDirect

Journal of Power Sources

journal homepage: www.elsevier.com/locate/jpowsour

Li-Ion polymer cells thermal property changes as a function of cycle-life

Hossein Maleki [a,*], Hsin Wang [b], Wally Porter [b], Jerry Hallmark [a]

[a] Motorola Mobile Devices, 1700 Belle Meade Court, Lawrenceville, GA 30043, USA
[b] Oak Ridge National Laboratory, One Bethel Valley Road, Oak Ridge, TN 37831, USA

HIGHLIGHTS

- 45 °C cycling impacts on thermal conductivity (K) of LIP cells were studied.
- Extended cycling at 45 °C reduces K-values of all LIP cells.
- K-values thought the thickness of the cell reduces more than along the length/width.
- In-plane K-values are dominated by the high K-values of current collectors.
- Current 4.35 V LIP cells have higher K-values than the past designed 4.2 V cells.

ARTICLE INFO

Article history:
Received 15 January 2014
Received in revised form
27 March 2014
Accepted 7 April 2014
Available online 19 April 2014

Keywords:
High voltage Li-Ion polymer cells
Thermal properties
Thermal conductivity
Si:C Li-Ion polymer cells
Thermal modeling

ABSTRACT

The impact of elevated temperature charge–discharge cycling on thermal conductivity (K-value) of Lithium Ion Polymer (LIP) cells of various chemistries from three different manufacturers was investigated. These included high voltage (Graphite/$LiCoO_2$:3.0–4.35 V), wide voltage (Si:C/$LiCoO_2$:2.7–4.35 V) and conventional (Graphite/$LiCoO_2$:3.0–4.2 V) chemistries. Investigation results show limited variability within the in-plane and through-plane K-values for the fresh cells with graphite-based anodes from all three suppliers. After 500 cycles at 45 °C, in-plane and through-plane K-values of the high voltage cells reduced less vs. those for the wide voltage cells. Such results suggest that high temperature cycling could have a greater impact on thermal properties of Si:C cells than on the LIP cells with graphite (Gr) anode cells we tested. This difference is due to the excess swelling of Si:C-anode based cells vs. Gr-anode cells during cycling, especially at elevated temperatures. Thermal modeling is used to evaluate the impact of K-value changes, due to cycles at 45 °C, on the cells internal heat propagation under internal short circuit condition that leads to localized meltdown of the separator.

1. Introduction

Demands for small form factor, light-weight, and high functionality portable electronic devices (e.g., notebooks, tablets, and smart phones) are growing dramatically. Depending on their mode of operation, these devices require batteries capable of handling power hungry applications, especially during long term operation under elevated temperatures. Because of their high energy density and long cycle life, Lithium Ion (Li-Ion) batteries are the primary choice for most of today's portable devices. These batteries' performance, never the less, relies highly on the thermal stability of their cells' chemistry, design and assembly quality, and most importantly the operating conditions, i.e., temperature and charge–discharge currents and voltage. Manufacturers are therefore challenged to build high thermal stability Li-Ion batteries to meet device performance requirements.

It is well known that temperature plays a critical role in the Li-Ion battery cycle-life. For this reason, most Li-Ion batteries are equipped with thermal control devices that limit their charge–discharge above 45 °C and 60 °C, respectively. Hence, low heat generation and high thermal conductivity (K) can play critical roles in the Li-Ion batteries long cycle-life. Variation in K-value is the key indicator of a Li-Ion battery's heat dissipation capability that changes with temperature rise. Changes in the K-values of Li-Ion batteries could depend on changes in cell properties such as:

- Electrode layers swelling during operation

* Corresponding author.
E-mail address: HosseinMaleki@motorola.com (H. Maleki).

http://dx.doi.org/10.1016/j.jpowsour.2014.04.033
0378-7753/

- Excess electrolyte reactions/loss and formation of thick SEI-layer over the anode
- Excess gas generation leading to loss of contact pressure and separation among separator and electrode layers as well as swelling of the cell packaging (pouch).

This article investigates the impact of 45 °C charge–discharge cycling on K-values of LIP cells of different sizes and chemistries from three major manufactures (A, B & C). Thermal simulations were used to determine impact of K-value changes, due to cycling at 45 °C, on heat propagation in fresh vs. cycled cells with graphite and Si:C-based anode materials from supplier-A. Fig. 1 shows a photo, and schematic of internal construction of a typical LIP cell.

2. Methods: experimental and computational

It is well known that direct thermal conductivity (K) measurement of Li-Ion cells with layered electrode structures is challenging and so there is a lack of such important data, particularly in open literature. Therefore, Li-Ion cell K-values are generally calculated by multiplying the values of density (ρ), thermal diffusivity (α) and specific heat (Cp) as noted in (Eq. (1)). The following two sections outline measurements of thermal diffusivity and specific heat, which are then used to calculate thermal conductivity using:

$$K = \rho\alpha \mathrm{Cp} \tag{1}$$

The α-values are generally measured using a laser or a Xenon-Flash Technique (XFT). For this work, we utilized the XFT facility at the High Temperature Materials Laboratory (HTML) of the Oak Ridge National Laboratory (ORNL). In XFT, the front face of a sample is subjected to a short pulse of Xenon light and the resulting temperature rise on the rear face of the sample is measured as a function of time using a photo-pyrometer. Given the sample thickness (L) and half-time of maximum temperature rise at the sample's rear face ($t_{1/2}$), thermal diffusivity is calculated using:

$$\alpha = \frac{1.38}{\pi^2}\left(\frac{L^2}{t_{1/2}}\right) \tag{2}$$

Derivation detail [1–3] for the α calculation is noted in the Appendix section of this article.

2.1. Thermal diffusivity (α) measurement

Fresh LIP cells of different sizes from manufactures A, B and C were discharged to 2.5 V at low current (0.1C) in order to avoid any thermal events during measurement. In-plane and through-plane α-values for stacked layers of each of the cell components were measured using XFT. Furthermore, additional fresh cells were first placed inside a convection oven with temperature set at 45 °C. The cells were cycled under the following conditions:

1 High voltage cells, charged to 4.35 V and discharged to 3.0 V at 1C
2 Si:C-anode cells, charged to 4.35 V and discharged to 2.7 V at 1C

Cells were cycled 500 times with a 5.0 min rest between each charge–discharge step and each charge step terminated when the charge current dropped below 20 mA.

Table 1 covers detailed information on the tested cells with their α-values. Fig. 2a shows schematic for stacked layers of a LIP cell, test sample, components and Fig. 2b details arrangements the components exposed to Xenon light during in-plane and through- plane α measurements.

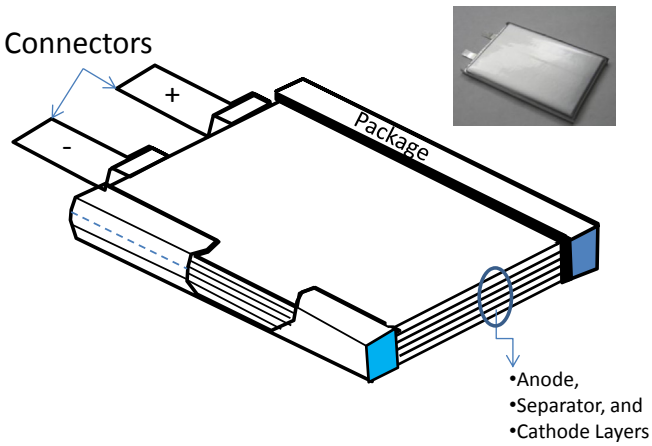

Fig. 1. Photo and schematic of a typical LIP cell.

2.2. Specific heat (Cp) measurement

Along with thermal diffusivity, the specific heat is used to calculate thermal conductivity. The specific heat can be determined in two ways: 1) using Differential Scanning Calorimeter (DSC); or 2) calculated based on empirical mass-fraction of *Cp* values for each of the cell components (anode, cathode, separator, electrolyte and packaging) using

$$\mathrm{Cp} = \frac{\sum (m\mathrm{Cp})_i}{\sum (m)_i} \tag{3}$$

[4], where m and Cp are the mass (g) and the specific heat [J (g °C)$^{-1}$] of the cell components. For validation reasons, we determined and compared the *Cp* value of a cell from supplier A using both the DSC and the Eq. (3) methods. The *Cp* values of the cells from suppliers B and C were determined using the Eq. (3) method.

2.3. Specific heat (Cp) using DSC analysis

A Q2000 DSC (TA Instruments, Delaware, USA) was used to determine the *Cp*-value of cell components: two 5.0 mm-diameter by 1.0 mm-thick disks were prepared by punching through the entire thickness of a cell (supplier-A); removing the outer pouch layer; and separating the remaining cell components into two approximately equal stacks of material layers (35.24 mg and 44.61 mg). A similar sized sample, containing the packaging materials only, was made by stacking eight disks of the packaging material (27.8 mg). Measurements were made in the temperature range from −100 to 40 °C. Hermetically sealed aluminum pans and lids were used during the DSC runs, and all runs were conducted in helium (He) flowing (5 sccm) environment. The maximum temperature of 40 °C was chosen to avoid deformation of the sealed sample pans from pressure buildup caused by volatilization of the electrolyte at higher temperatures. Heating and cooling rates of 20 °C min^{-1} were used. The measurements were made using the three run ratio method described in ASTM E1269 [5]. The standard reference material was a synthetic sapphire disk that had a total heat capacity that closely matched that of the specimens under test. At the same time the cell materials were measured a specimen of NIST SRM 781 Molybdenum was measured to determine the system accuracy. The Cp-value of the Molybdenum calculated from the heating cycle data were found to be 5–6% higher than the NIST certificate values, while those for cooling were 2% high. For this reason, Cp-values calculated only from the cooling cycle results are reported here. The uncertainty of the Cp-value results is estimated

Table 1
Li-Ion test cells' properties and their associated in-plane and through-plane thermal conductivity (fresh and after 500 cycles at 45 °C).

Cell manufacturers	Cell chemistry	Cell condition	Operation voltage (V)	No. of samples	Ave. Density g (cm^{-3})	Specific heat J $(g\ °C)^{-1}$		Thermal diffusivity $cm^2\ s^{-1}$		Thermal conductivity W $(m\ K)^{-1}$	
								Through- plane	In-plane	Through- plane	In-plane
A	High Voltage (Gr/LCO)	Fresh	3.0–4.35	4	2.51	1.028	Value	0.00633	0.1433	1.63	36.96
							St. Dev.	0.00088	0.0145	0.23	0.23
		Cycled	3.0–4.35	4	2.31	1.028	Value	0.00585	0.1450	1.39	34.43
							St. Dev.	0.00100	0.0109	0.24	2.59
B	High Voltage (Gr/LCO)	Fresh	3.0–4.35	2	2.42	0.980	Value	0.00570	0.136	1.35	32.31
							St. Dev.	0.00212	0.001	0.50	0.27
		Cycled	3.0–4.35	2	2.25	0.980	Value	0.00645	0.1360	1.42	29.99
							St. Dev.	0.00219	0.0140	0.48	3.09
A	Wide Voltage (Si:C/LCO)	Fresh	2.7–4.35	2	2.51	0.990	Value	0.00480	0.1604	1.19	39.90
							St. Dev.	0.00053	0.0087	0.13	2.17
		Cycled	2.7–4.35	2	2.18	0.988	Value	0.00390	0.1500	0.84	32.31
							St. Dev.	0.00014	0.0120	0.03	2.58
C	St. Voltage	Fresh	3.0–4.2 V	4	2.36	0.986	Value	0.00510	0.1398	1.19	32.52
							St. Dev.	0.00014	0.0015	0.03	0.35

Notations: Gr (Graphite), Si (Silicon), LCO ($LiCoO_2$), and C (Carbon).

to be less than 3%, which is typical for the method used. Finally, Cp-value of each sample was determined using

$$\mathrm{Cp}(s) = \mathrm{Cp}(st)\frac{Ds}{Dst}*\frac{Wst}{Ws} \tag{4}$$

Cp(s): specific heat of the sample J $(g\ K)^{-1}$,
Cp(st): specific heat of the sapphire standard J $(g\ K)^{-1}$,
Ds: vertical displacement between the sample holder and the sample DSC thermal curves at a given temperature (mW),
Dst: vertical displacement between the sample holder and the sapphire DSC thermal curves at a given temperature (mW), and
Ws: mass of sample (mg)
Ws: mass of sapphire standard (mg).

Fig. 3 shows plots of DSC data on cooling direction for the two sets of the cell's samples of electrodes and separators, the packaging material and the Molybdenum NIST-SRM. Because the entire thickness of the cell sample could not fit into a sample holder (pan), and the two stacks of layers might have different numbers of cell component layers, the Cp-value was determined in two parts. Then, the cell's effective Cp-value was calculated using the mathematical relation below (expanded version of Eq. (3)):

$$\mathrm{Cp} = \frac{\sum(\mathrm{mass}*\mathrm{Cp})_{\mathrm{sample}-1} + (\mathrm{mass}*\mathrm{Cp})_{\mathrm{sample}-2} + (\mathrm{mass}*\mathrm{Cp})_{\mathrm{Package}}}{\sum\left(m_{\mathrm{sample}-1} + m_{\mathrm{sample}-2} + m_{\mathrm{package}}\right)}. \tag{5}$$

Table 2 covers Cp-values of type-A cell components and the effective cell Cp-value.

2.4. Specific heat (Cp) calculation using weighted mass-fraction of the cell components

1. Discharged cells to 2.5 V at 0.1C (stop when current dropped below 20 mA).
2. Each cell mass was weighed and then dissected.
3. Cells' components were washed using Dimethyl-carbonate (DMC) solvent and vacuum dried for 48 h.
4. Masses of cells' components were measured after vacuum drying step.
5. Difference in total mass of an unassembled cell before and dissembled parts after washing and vacuum drying provided electrolyte mass information.
6. Cells' electrode binder material mass data were provided by the cell suppliers.

Table 3 shows details of the cell individual component masses with their associated Cp values. Type A cell Cp-value [1.028 J $(g\ °C)^{-1}$] was calculated using Eq. (3). Note that the calculated Cp value is about 25% higher than the Cp-value [0.824 J $(g\ °C)^{-1}$] of the same cell sample measured using DSC. Such difference must be related to electrolyte loss due to package removal followed by some waiting period before testing of the samples.

Overall analysis results show that Cp-values of these cells are close to [1.0 J $(g\ °C)^{-1}$]. Such results should come as no surprise since most suppliers are using nearly the same design parameters (noted below) to build LIP cells with comparable volumetric energy density in order to compete for mobile devices applications. Typical recent cell design parameters are:

- 110–120 μm thick $LiCoO_2$-based cathodes including 15–16 μm thick aluminum current collector.
- 120–130 μm thick graphite-based anodes including 10–11 μm thick copper current collector.
- 15–16 μm thick polyethylene- based separator.
- 85–90 μm thick packaging consists of 35–40 μm thick aluminum foil laminated between oriented nylon and polypropylene (PP) layers.
- Any three/four combinations of organic solvents [Ethylene carbonate (EC), Di- methyl carbonate (DMC), with Ethyl-methyl carbonate (EMC), and/or Diethyl-carbonate (DEC)] with lithium salts (typically $LiPF_6$).

Previous design Li-Ion cells' anode and cathode (150–160 μm) and separator (20 μm) were thicker than those for the current cell design. Such difference translates to a thicker previous design cell

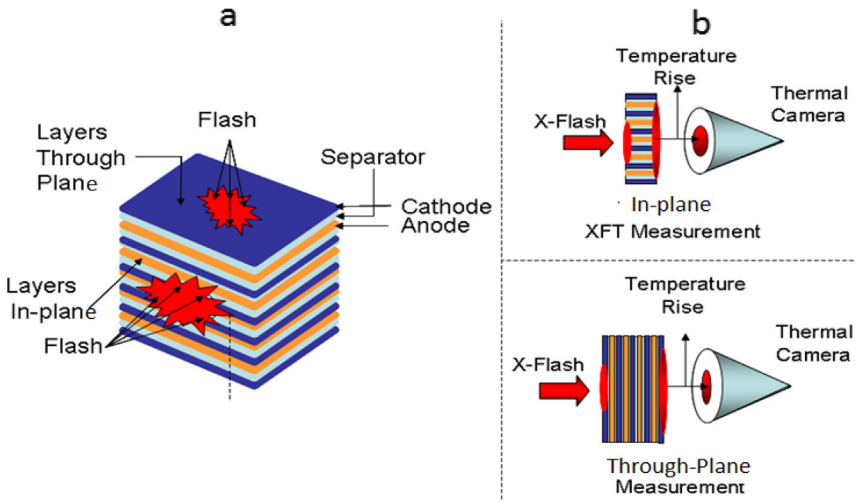

Fig. 2. Schematic of Xenon Flash Technique. Energetic light is shined over the front face of the stacked cathode/separator/anode layers and then half-time of maximum temperature rise on the sample is measured using a high speed thermal camera.

with different thermal properties than the current design cell with both having similar volumetric energy density (Wh l^{-1}).

2.5. Thermal modeling

It is known that separator defects or localized meltdown in Li-Ion cells leads to internal short circuit (ISCr). The ISCr may lead to thermal runaway if the separator meltdown propagates such that large areas or number of anode and cathode layers are touching each other [6,7]. Obviously, the risk of thermal runaway from ISCr increases when the ISCr surrounding temperatures approach the decomposition reaction temperature of cathode with electrolyte which varies with material type and state of charge [8]. In this article we have investigated the impact of thermal conductivity changes, due to cycling at 45 °C, on temperature rise and propagation in a generic LIP cell (6 × 48 × 68 mm) with graphite or Si:C-based anode material having similar properties as type-A cell.

Modeling conditions included:

- Cell structure treated as a lumped system,
- Natural convection cooling under 25 °C ambient,
- A hot-spot (1.0 × 1.0 × 1.0 mm, 20 W) positioned at the center of the cell. The 20 W hot-spot is to create a localized temperature rise to near melting point (135 °C) of the typical separator (PE with no ceramic coating) in <1.0 s, and
- Transient heating (1–60 s) covering temperature rise for typical LIP cells under ISCr.

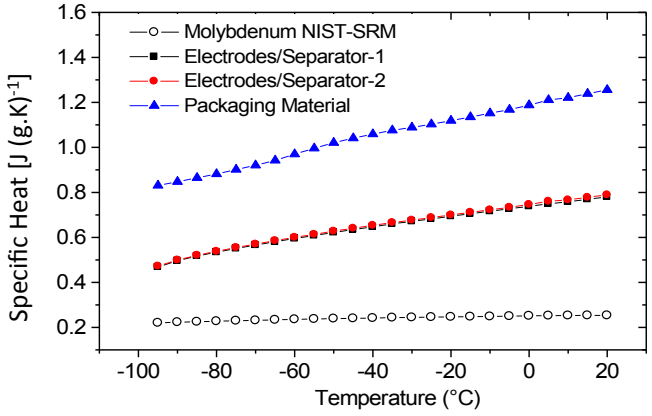

Fig. 3. Plots of the specific heat values of the Molybdenum, cell packaging material, and electrodes and separators samples.

3. Results and discussions

We have determined the impact of high temperature charge–discharge cycling (500 times at 45 °C) on the thermal conductivity (K) of high voltage (3.0–4.35 V, Graphite/$LiCoO_2$), wide voltage (2.75–4.35 V, Si:C/$LiCoO_2$) and conventional (3.0–4.2 V) Li-Ion Polymer (LIP) cells. Table 1 provides a summary of the tested cells' information with their associated specific heat (Cp), thermal diffusivity (α) and thermal conductivity (K) values. Results show:

1 Due to similarities in design and materials properties, the Cp-values of all tested LIP cells are close to 1.0 J (g °C)$^{-1}$.
2 Effective K-values of these LIP cells are dominated by their higher in-plane K-values than the through-plane K-values. In this case, the higher in-plane K-values must be attributed to the much higher K-values of the anode's copper [400 W (m K)$^{-1}$] and cathode's aluminum [240 W (m K)$^{-1}$] current collectors than their coating materials.
3 The cells' through-plane K-values varies depending on the impacts of cycling on the cells' stability vs. swelling and/or loss of stack pressure among electrodes, separator, and cell packaging layers. Under extended charge–discharge cycling, Li-Ion/LIP cell swelling is partially related to: 1) formation of gaseous byproducts from repeated cathode and anode reactions with electrolyte, and 2) anode thickness increase due to lithium insertion-extraction process [9–11]. Our test results (unpublished data) on cells from many manufacturers have also shown that extended cycling leads to swelling of Li-Ion/LIP cells with stiffening (or even deformation) of the anode. Such changes,

Table 2
Cp value of type-A cells obtained using DSC analysis.

Samples	Cp J (g °C)$^{-1}$	Mass (mg)	Mass*Cp J (°C)$^{-1}$	$Cp = \frac{\sum (mCp)_i}{\sum (m)_i}$
Electrodes/Seprator-1	0.781	35.24	27.53	0.824 J (g °C)$^{-1}$
Electrodes/Seprator-2	0.790	44.61	35.22	
Packaging	1.256	6.95	8.73	

Table 3
Examples of high and wide voltage LIP cells *Cp*-value calculation using cells' components mass fractions.

Materials	Supplier-A/HV Cell (3.0–4.35 V)			Supplier-A/WV Cell (2.7–4.35 V)			Supplier-C Convential Cell (3.0–4.2 V)		
	Mass (g)	Cp J (g °C)$^{-1}$	Cp*Mass J (°C)$^{-1}$	Mass (g)	Cp J (g °C)$^{-1}$	Cp*Mass J (°C)$^{-1}$	Mass (g)	Cp J (g °C)$^{-1}$	Cp*Mass J (°C)$^{-1}$
Cathode ($LiCoO_2$)	12.024	0.849	10.21	12.02	0.849	10.21	14.20	0.85	12.06
Aluminum Foil	1.22	0.9	1.09	1.48	0.9	1.33	1.29	0.90	1.16
Anode (Graphite)	5.87	0.693	4.07	5.58	0.693	3.87	6.30	0.69	4.37
SiO2	N/A	N/A	N/A	0.21	0.712	0.15	N/A	N/A	N/A
Copper Foil	3.61	0.385	1.39	3.47	0.385	1.34	3.01	0.39	1.16
Separator (PE)	2.52	2.31	5.82	1.15	2.31	2.66	1.30	2.31	3.00
Pouch (Nylon/Al/PP)	1.92	1.25	2.41	1.17	1.71	2.00	1.00	1.71	1.71
Electrolyte*	3.84	1.64	6.29	3.10	1.64	5.09	4.30	1.64	7.05
Additive Carbon	0.38	0.716	0.27	0.37	0.716	0.26	0.30	0.716	0.21
Binder (PVDF)	0.98	1.77	1.73	0.95	1.77	1.68	0.70	1.77	1.24
	Total Mass		Sum: (Cp*Mass)	Total Mass		Sum: (Cp*Mass)	Total Mass		Sum: (Cp*Mass)
	32.36		33.3	29.5		29.15	32.40		31.96
Σ (Cp*Mass)i/Σ(mass)i	Cp = 1.028 J (g °C)$^{-1}$			Cp = 0.988 J (g °C)$^{-1}$			Cp = 0.986 J (g °C)$^{-1}$		

obviously, have greater impacts on the through-plane than the in-plane K-value of LIP cells that are mostly dominated by the high K-values of their cathode and anode current collectors. Therefore, Li-Ion/LIP cell manufacturers are obligated to provide swelling vs. cycle-life data for the battery end users or product designers.

4 Cycling at 45 °C reduces the in-plane K-values of the high voltage type A and B cells by 7% and type-A wide voltage cells by 20%. For through-plane, K-values of the high and wide voltage type-A cells reduce by 15 and 30%, respectively. The high voltage type-B cells through-plane and the in-plane K-values reduce by 5.0% and 7%, respectively.

Note that the through- and in-plane K-values of the fresh type-A high voltage (4.35 V) cells are about 37% and 14%, respectively, higher than those for the type-C standard voltage (4.2 V) cells. Such results are indicative of more efficient component packing in the new high energy density/voltage cells vs. standard cell (4.2 V) designs. Efficient packaging includes application of electrodes, optimized for the highest possible energy density and thermal conductivity, and the thinnest possible separator layers with good adhesion and/or stack pressure between them and the cell packaging. Such design, in a given LIP cell, allows incorporation of more electrode layers that could transfer heat faster due to a higher number aluminum and copper current collectors. Thermal modeling, in the sections below, is used to demonstrate the role of the electrodes and separator thickness in temperature rise of LIP cells.

The lower through-plane K-values of type-A Si:C-anode based cells vs. others cells must be attributed to their excess swelling due to high gas generation of the Si:C-anode because of cycling, especially under elevated temperature. It is well known that Si has the highest known theoretical charge capacity (4200 mAh g^{-1}) among anode materials (>10 times of graphite, 375 mAh g^{-1}). Si:C-anode application, however, is hindered because of the large volume expansion (400%) and contraction of Si during charge and

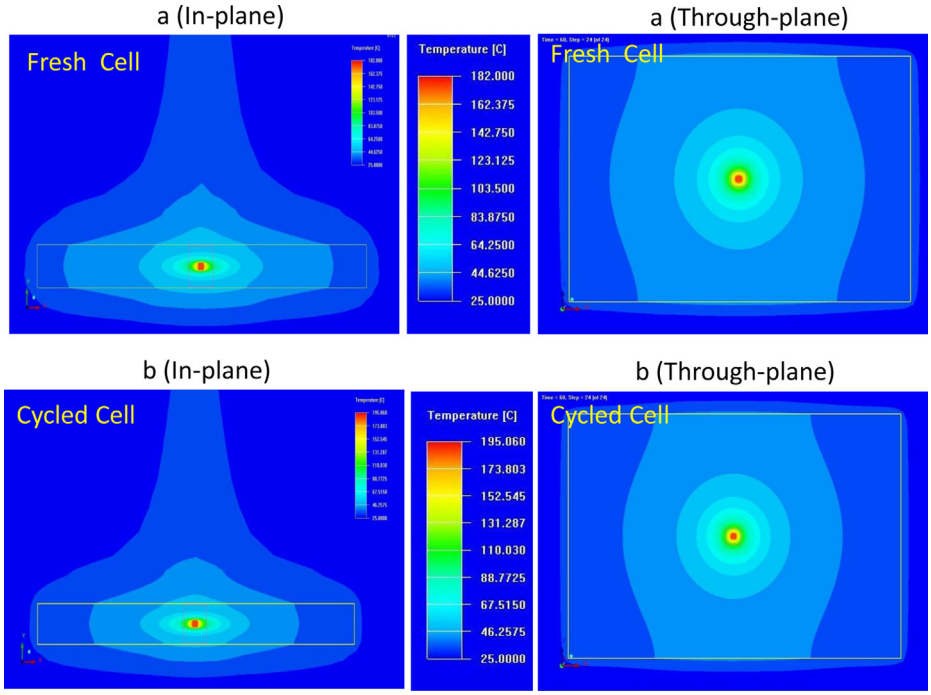

Fig. 4. In-plane and through-plane thermal profiles of a generic LIP cell (6 × 48 × 68 mm), before and after 500 cycles at 45 °C. Cycling led to 13 °C higher temperature after 60 s of exposure to a hotspot with 20 W power dissipation.

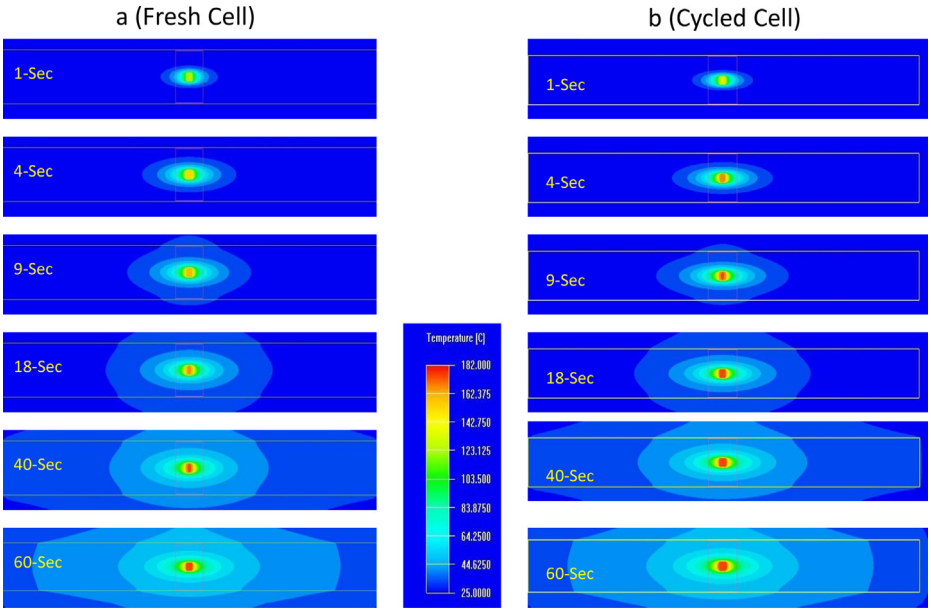

Fig. 5. Through-plane thermal profiles of a generic LIP cell (6 × 48 × 68 mm), fresh and after 500 cycles, during 60 s exposure a to hotspot with 20 W power dissipation. The cycled cell internal temperature increases faster (growth in red color intensity) than the fresh cell. (For interpretation of the references to colour in this figure legend, the reader is referred to the web version of this article).

discharge, respectively. In this case, the large volume change results in cracking of the Si structure. The extended charge–discharge cycling leads to further fracturing and destruction of Si particles, causing deterioration of adhesion networks and separations among the anode particles and current collectors [12]. This process leads to additional reactions of the broken anode materials with electrolyte to form new solid-electrolyte-interface (SEI) layers that leads to formation of gaseous byproducts including CO_2, CO and CH_4 [10–13]. Accumulation of gases due to repeated SEI-layer formation and resulting deformation of the anode layers leads to excess swelling of the Si:C-anode based cells vs. graphite anode cells that do not suffer severe volume change under extended charge–discharge cycles. Furthermore, the Si-anode severe volume expansion and contraction increases capacity fade rates of Li-Ion cells, depending on their discharge voltage [14]. These are the reasons that major manufacturers have delayed their Si-anode based Li-Ion cells/batteries production for the mass markets in the last few years. These manufacturers, however, continue searching for suitable combinations of binder material, Si:C coating process and electrolytes-additives recipes that combat the high capacity fade and swelling of Si-anode based Li-Ion cells. On this note, some manufacturers have commercialized a small number of Si-anode based Li-Ion/LIP cells with Si-to-C ratio of less than 6.0% for a very limited portion of the globally available Li-Ion batteries market.

A review of work on Si-anode issues indicates efforts focused on changes to electrolyte or binder compositions. Chen et al. showed positive impacts of vinylene carbonate (VC) as electrolyte additive on electrochemical performance of Si-anode for Li-Ion batteries [15]. They concluded that presence of VC in electrolyte brings out

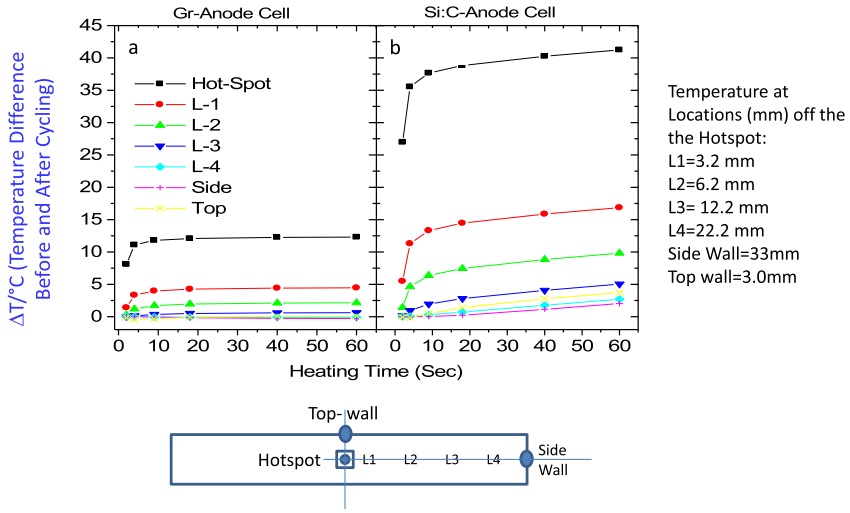

Fig. 6. Localized temperature rise difference for the high (Gr-anode) and wide (Si:C anode) voltage generic cells (6 × 48 × 68 mm), before and after 500 cycles at 45 °C, at various points away from the hotspot.

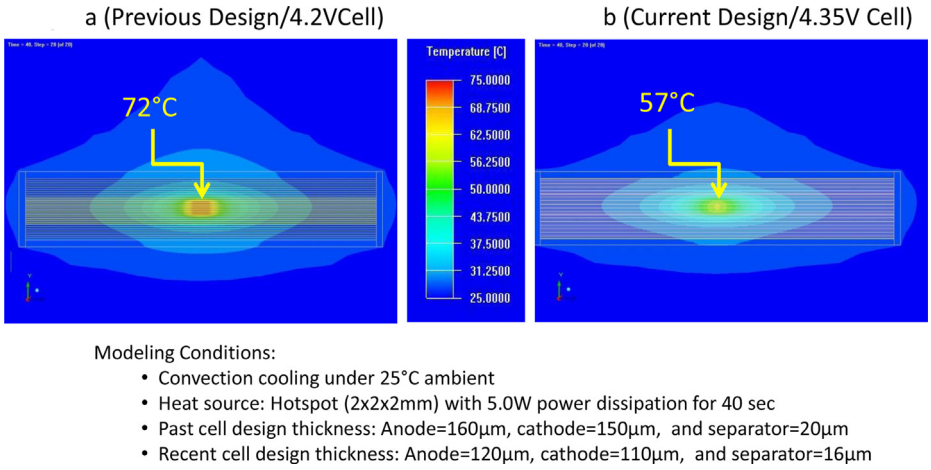

Fig. 7. Thermal profiles for a generic LIP cell using the new high voltage Type-A cell design vs. cell design from the past. Due to thicker electrodes and separator, the past designed cell temperature increases faster than that for the current cell design-red color is indicative of higher temperature. (For interpretation of the references to colour in this figure legend, the reader is referred to the web version of this article).

the VC-reduced products and decreased the LiF content in SEI-layer. Bordes et al. demonstrated that addition of 5.0% fluoroethylene carbonate (FEC) to the ethylene carbonate-diethyl carbonate based electrolytes improves capacity and cycle-life of Li-Ion cells consisted Si:C anode and $LiNiCoAlO_2$ cathode [16]. They noted that improvement is due to formation of a thin (30–50 nm) SEI-layer with low ionic resistance (~2 ohm cm^2) on the surface of Si:C anode. Inose et al. examined the influence of electrolyte solutions on charge–discharge properties of Si-based anodes [17]. They concluded that cycling-life degradation of Li/Si:C based cells is due to breakdown of electronic conductive path of Si-anode resulting from a large volume change of Si during charge–discharge. Kim et al. showed that polyimide (PI) provides a higher stability and recuperative capability than poly-vinylidine difluoride (PVDF) binder vs. volume expansion and contraction of Si-anode based Li-Ion batteries [18]. Choi et al. showed that polyamide (PAI) based binder is a much more effective restraint on volume expansion in active Si materials during the charging process than PVDF binder [19].

Fig. 4a and b shows the thermal profile of a generic cell with similar properties as the type-A high voltage cells, fresh and cycled, after 60 s of exposure to a hot-spot with 20 W power dissipation. Note that the hotspot temperature for the cycled cell increases ~13 °C higher than the fresh cell. This indicates that changes in parameters (K, α and ρ values) in a Li-Ion/LIP cell, due to cycling, increase thermal rise of a battery that ultimately leads to high heat accumulation in the host device, i.e., cell phones with plastic housing having limited heat dissipation capability due to the low K-values the housing materials, typically <0.5 W $(m\ K)^{-1}$.

Fig. 5a and b shows thermal profiles of the same type-A LIP generic cells as a function of time. For clarity, the cycled cell maximum temperature is set the same as the fresh cell maximum temperature (182 °C). Note that the hot spot temperature for the cycled cell increases faster than the fresh cell, illustrated by the higher "red color" intensity indicating higher temperature.

Fig. 6a and b shows difference in temperature rise for a generic type-A high (Gr-anode) and wide (Si:C-anode) voltage cells, fresh and cycled, during 60 s exposure to the 20 W hotspot. The simulation results show that the difference in temperature rise for the cycled vs. fresh wide voltage cell are much higher than those for the high voltage cell. So, consideration of cycling impacts on thermal behavior of Si-anode based batteries vs. cycling is important for application of this battery technology in portable devices' heat management, particularly for those with housing materials having limited heat dissipation capability.

Fig. 7 shows thermal simulation results on high voltage (4.35 V) vs. standard voltage (4.2 V) LIP cells of the same size but different component design parameters, both under a hotspot with 5.0 W power dissipation for 40 s. The 4.20 V cell includes 28 anodes, 29 cathodes and 30 separators layers with each anode, cathode and separator layer being 160, 150 and 20 μm, respectively. The 4.35 V cell includes 38 anodes, 39 cathodes and 40 separators layers with each anode, cathode and separator layer being 120, 110 and 16 μm thick, respectively. This is to demonstrate the importance of component design parameters in a LIP cell heat transfer vs. events such as localized internal short circuit (ISCr). In this case, the high voltage 4.35 V LIP cell (Max Temp. 57 °C) with a higher number of electrodes has less risk of going to thermal runaway vs. the 4.2 V LIP cell (Max Temp. 72 °C) with a lower number electrodes. However, good control of the heat conduction in the through-plane direction is highly critical due to swelling effects; and/or when ISCr spot temperature reaches near the separator melting point (i.e., 130 °C for polyethylene).

4. Conclusion

The impact of elevated temperature charge–discharge cycling on thermal conductivity (K-value) of Lithium Ion Polymer (LIP) cells of various chemistries from three different manufacturers was investigated. Results show that the in-plane and through-plane K-values of the new high voltage LIP cells are ~25% higher and ~50% lower, respectively, than those for cells we examined in 1999 [4]. Such difference, vs. the old designed cells, is achieved through applications of more layers of thinner (~20%) separator and thinner anode (25%) and cathode (27%) with materials coatings designed for optimum energy density. Today's high voltage (4.35 V) Li-Ion/LIP cells energy density (550–600 Wh L^{-1}) are ~30% higher than those for conventional cells (4.2 V) from the past.

Swelling due to extended cycling at elevated temperature (45 °C) reduces thermal properties of LIP cells with greater impact on the through-plane K-value than the in-plane K-value. LIP cells' effective thermal conductivity is mostly dominated by the in-plane K-values due to contribution from high K-values cathode aluminum and anode copper current collector layers.

The new Si:C-anode based LIP cell's excess swelling during cycles at 45 °C led to its lower K-values than the Gr-anode based LIP

cell. Therefore, such behavior could play a critical role in heat management of devices using the Si:C-anode based LIP battery chemistry that could offer much higher energy density than conventional Gr-anode based chemistry.

Finally, changes in cell construction (e.g., swelling, and/or separation among components), reduces LIP cells thermal conductivity (K). This reduction of the K-value ultimately increases risks of abnormal thermal events, especially in case of internal short conditions that lead to large areas of separator melting propagation.

Authors comments

For confidentially reasons, the cell suppliers' names and details of the cells' size and capacity values are not discussed. All tests were conducted on cells components that were reassembled after partial disassembling. Therefore, application of the thermal conductivity (K-values) data provided in this article may not provide representative thermal modeling/evaluation results for all LIP Li-Ion cells, especially since the high temperature cycling impacts on LIP cells could vary with testing condition and suppliers.

Acknowledgement

Authors would like thank Inna Kerzhner-Haller (Motorola Mobility Products Safety) for testing the cells cycle-life at 45 °C. This work was supported in part by the Assistant Secretary for Energy Efficiency and Renewable Energy, Office of Vehicle Technologies of the U.S. Department of Energy.

List of symbols

B_t	dimensionless number for transient diffusion, Eq. (A-4)
Cp	specific Heat, J (g °C) $^{-1}$
K	thermal conductivity, W (m K)$^{-1}$
Q	light energy pulse density, J (m^2)$^{-1}$
t	time, sec
t_c	characteristic time for diffusion, sec
V	dimensionless temperature rise, Eq. (A-4)
α	thermal diffusivity, m^2 s^{-1}
m	sample mass (g)
ρ	density [g (cm^3)$^{-1}$]

Appendix

The thermal diffusivity equation covering Xenon Flash Technique (XFT) is based on the classical heat conduction solution described in parts in Refs. [1–4]. The basic theory underlying the XFT is governed by the three-dimensional Eq. (A-1) of heat diffusion in the sample:

$$\alpha \nabla^2 T = \frac{\partial T}{\partial t} \tag{A-1}$$

with temperature (T) being a function of time (t) and position (x). Assuming a finite slab of thickness L with a large area, uniformly illuminated without any heat loss from the side and rear surfaces, heat conduction becomes one dimensional and the transient temperature is $T(x, t)$. If the input energy pulse duration is much shorter than the characteristic time of the temperature transient from the front to the rear face of the sample, then the exact solution of Eq. (A-1) can be replaced by the analytic solution for an instantaneous pulse. Parker et al. [1] have shown that the temperature rise at the sample rear face ($x = L$) is

$$T(L,t) = \frac{Q}{C_p \rho L}\left[1 + 2\sum_{n=1}^{\infty}(-1)^n \exp\left(\frac{-\alpha n^2 \pi^2}{L^2} t\right)\right] \tag{A-2}$$

Here, Q is the pulse energy density (J m^{-2}) shined on the front face of the sample; Cp is the specific heat; and ρ is the density of the sample. For samples less than 3 mm thick and of moderate thermal diffusivity, the pulse duration should be less than 10% of the characteristic diffusion time. From Eq. (A-2), the characteristic diffusion time, t_c is $t_c = L^2/\pi^2\,\alpha$, and the maximum temperature rise, $T_{L,\max}$, at the rear face of the sample is

$$T_{L,\max} = \frac{Q}{C_p \rho L}. \tag{A-3}$$

At any time $t > 0$, the temperature rise at the rear face of the sample as a fraction of its maximum temperature rise is

$$V = 1 + 2\sum_{n=1}^{\infty}(-1)^n \exp\left(-\pi^2 n^2 B_t\right) \tag{A-4}$$

Here V, the normalized temperature rise, is defined as $T(L,t)/T_{L,max}$, and $B_t = \pi^2 \alpha t/L^2$. From Eq. (A-4) it follows that if $V_x = 1/2$, then $B_t = \pi^2 \alpha t/L^2 = 1.38$. Thus the half-time of the temperature rise, $t_{1/2}$, can be used to determine α

$$\alpha = \frac{1.38}{\pi^2}\left(\frac{L^2}{t_{1/2}}\right) \text{ or } = 0.1338\left(\frac{L^2}{t_{1/2}}\right) \tag{A-5}$$

References

[1] W.J. Parker, R.J. Taylor, C.P. Butler, G.L. Abbot, J. Appl. Phys. 32 (1961) 1679.
[2] R.E. Taylor, K.D. Maglic, in: K.D. Maglic, A. Cezairliyan, V.E. Peletsky (Eds.), Compendium of Thermophysical Property Measurement Methods: Survey of Technique, Plenum Press, New York, 1984, p. 305.
[3] L.M. Clark III, R.E. Taylor, J. Appl. Phys. 46 (1975) 714.
[4] R.F. Bulmer, R. Taylor, High. Temp. High. Press. 6 (1974) 491.
[5] H. Maleki, S. Al Hallaj, J.R. Selman, R.B. Dinwiddie, H. Wang, J. Electrochem. Soc. 146 (3) (1999) 947–954.
[6] ASTM International, West Conshohoken, PA, 2011.
[7] W. Cai, H. Wang, H. Maleki, J. Howard, E. Lara Curzio, J. Power Sources 196 (2011) 7779–7789.
[8] H. Maleki, J.N. Howard, J. Power Sources 191 (2009) 568–574.
[9] N. Zhang, H. Tang, J. Power Sources 218 (2012) 52–55.
[10] J.S. Shin, C.H. Han, U.H. Jung, S.I. Lee, H.J. Kim, K. Kim, J. Power Sources 109 (2001) 47–52.
[11] W. Kong, H. Li, X. Huang, L. Chen, J. Power Sources 142 (2005) 285–329.
[12] T.D. Bogart, A.M. Chockla, B.A. Korgel, Curr. Opin. Chem. Eng. (2013) 286–293.
[13] S.E. Sloop, J.B. Kerr, K. Kinoshita, J. Power Sources 119–121 (2003) 330–337.
[14] P. Hovington, M. Dontigny, A. Guerfi, J. Trottier, M. Lagacé, A. Mauger, C.M. Julien, K. Zaghib, Curr. Opin. Chem. Eng. 248 (2014) 457–464.
[15] L. Chen, K. Wang, X. Xie, J. Xie, J. Power Sources 174 (2007) 538–543.
[16] A. Bordes, K. Eom, T.F. Fuller, J. Power Sources 257 (2014) 163–169.
[17] T. Inose, D. Watanabe, H. Morimoto, S. Tobishima, J. Power Sources 162 (2) (2006) 1297–1303.
[18] J.S. Kim, W. Choi, K.Y. Cho, D. Byun, J.C. Lim, J.K. Lee, J. Power Sources 244 (2013) 521–526.
[19] N.S. Choi, K.H. Yew, W.U. Choi, S.S. Kim, J. Power Sources 177 (2008) 590–594.